

Dilute nitride lasers and non-equilibrium phonon populations

Chapter 7

7.1 Introduction

In this chapter, the thermal model developed in Chapter 5 is extended to include the impact of non-equilibrium LO-phonons generated via QW carrier relaxation. The strong LO-phonon/carrier interaction, coupled with the finite LO-phonon decay time, results in a hot-phonon population being formed around the QW. This in turn elevates the QW carrier temperature far above that of the lattice. The impact of the hot phonon population (or phonon bottleneck) on the transient response and the light-current (L-I) characteristics of the device are studied. It is found that the LO-phonon bottleneck is particularly large in dilute nitride devices because of the large conduction band offset.

At moderate injection currents, the hot phonon population is found to increase the carrier temperatures in the QW by up to 7K above that of the equilibrium lattice temperature. At high injection currents, the phonon bottleneck can significantly decrease the optical power.

7.2 The LO-phonon bottleneck

Before the bulk 3D carriers can reach the lasing states, they must first be captured into

the confined 2D energy states at the top of the QW. In terms of energy, there is a considerable difference between the 2D states at the top of the QW and those at the bottom (near the lasing states). As the carriers relax inside of the QW, they lose energy and momentum. At room temperature, the dominant scattering mechanism for carriers in GaAs-type semiconductors is carrier/LO-phonon scattering. Thus, as carriers relax in the QW, a large number of LO-phonons are generated. The process of carrier capture and relaxation is depicted in figure 7.1.

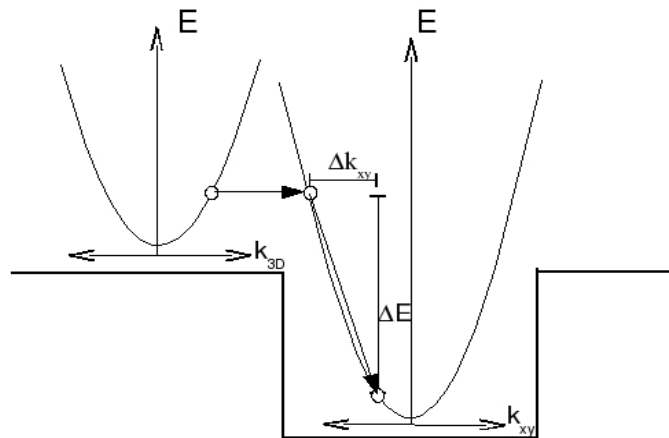


Figure 7.1: Capture of carriers to lasing states.

LO-phonons have a low phase velocity due to their flat dispersion curve (see figure 7.2). Thus, they cannot propagate away from the QW. Finally, a large population of LO-phonons can build up around the QW, due to their finite decay time. Due to the strong LO-phonon/carrier scattering mechanism, the hot LO-phonon population elevates the temperature of the carrier population. This spreads out the energy distribution of the carriers and decreases the material gain.

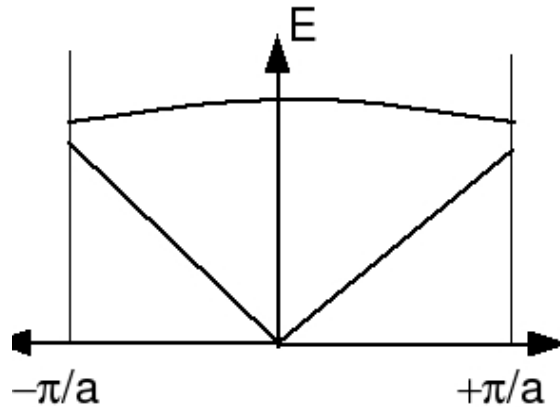


Figure 7.2: Dispersion relations.

The carrier/phonon problem can be modelled by treating the carrier populations as a gas. Injected electrons heat the carrier gas, which continually relaxes towards equilibrium with the lattice via LO-phonon emission. This can be represented using a rate equation model, with one rate equation for the energy of each population - electrons, holes, LO-phonons and equilibrium lattice phonons. These rate equations are solved for the electron, hole and LO-phonon temperatures.

7.3 Hot phonon models in the literature

Early rate equation models used to describe laser diodes neglected the impact of non-equilibrium LO-phonons [1,2]. In 1993, Tsai [3] considered the impact of hot-phonons in QW laser diodes. In this work, the lattice heat conduction equation was solved along with the carrier coupled photon rate equations, electron/hole temperature rate equations and an LO-phonon rate equation. This model was the first to make the following assumptions:

- Each confined carrier has an energy of kT (from 2D partition principal).
- Phonons were modeled as relaxing towards the hot carrier gas rather than the

carrier gas relaxing towards the phonon population.

- The LO-phonon dispersion curve was assumed flat.

However, carrier temperatures of over 480K were predicted, for lattice temperatures as low as 320K.

In 1996, the work was extended [4] using scattering times calculated from first principles as a function of \mathbf{k} -vector and temperature. The *piezoelectric acoustic phonon*, *deformation potential acoustic phonon*, *deformation potential optical phonon*, and *polar optical phonon (POP)* scattering times were evaluated. It was found that at room temperature, POP scattering dominates the carrier relaxation processes and only a small energy range of LO-phonons with \mathbf{k} -vectors between $3 \times 10^7 \sim 10^9 \text{m}^{-1}$ are excited. In the same year, Yu included a [5] LO-phonon rate equation in a VCSELs model. In 1999, Tsai further extended the model to include hole/TO-phonon scattering [6]. Monte-Carlo simulation has been used to investigate the phonon bottleneck and validate the rate equation models. Under strong lasing conditions, the rate equation approach and the Monte-Carlo approach give comparable results. This is because the FD distribution still remains in quasi-equilibrium under strong lasing conditions. The need for proper time constants and accurate broadening functions was underlined. Crucially, this work neglected lattice heating, which led to the underestimation of scattering times.

Matt Grupen (1998) [7] was the first to include the hot phonon effect in a full and extensive device simulator. He appreciated that momentum is not always conserved

normal to the plane of the QW, thus the range of states with which the phonons can interact is broadened. A complex capture escape model was introduced, which discretised the energy space in the QW and included intrasubband scattering. Later, Liu [8] used the model developed by Grupen to model the LO-phonon bottleneck in VCSELs. It predicted carrier temperatures to be 20K above that of the lattice temperature, whereby the LO-phonon decay time was used as a phenomenological fitting parameter to adjust the simulation to experiment.

Models previously described in the literature, have either been too simple to contain an accurate representation of the fundamental device physics [1-6] or introduce a large numerical overhead making them too complex and for day-to-day device design and optimisation [7-8]. In this chapter, hot carrier and hot LO-phonon effects will be included into the device simulator developed in Chapter 5. Throughout, the priority will be to minimise the computational overhead whilst retaining all the key elements of the physics associated with the model. The result is a model which is significantly more accurate than the traditional quasi-equilibrium models used to model carriers in the QW. At the same time, the model is more computationally efficient than these more complex models.

7.4 The model

One of the failings of the more simple models is the assumption that carriers in all the bands of the QW behave as a 2D gas and thus all have kT worth of kinetic energy (from partition theory). For a highly degenerate gas, as in the QW of a laser diode,

this assumption clearly does not hold. The non-parabolic nature of the valance band also makes this assumption questionable. Another failing of the more simple models is the assumption that all carriers, whether recombining radiatively or non-radiatively, relax to the same energy in the QW. This energy is often taken as the very bottom of the lowest band in the QW. This is also a questionable assumption because the lasing energy is slightly above the bottom of the band. Furthermore, the average carrier energy is far above the bottom of the band. By assuming that the carriers relax further than they do in reality before they recombine, the number of LO-phonons being generated is overestimated.

On the other hand, more complex simulators model the microscopic relaxation of carriers down the well and discretise the QW states in energy space. This approach leads to a significant computational overhead. Even in these more complex models [7-8], it is often assumed that the electron and hole temperatures are the same, thus neglecting the complex carrier relaxation energy pathways (see figure 7.3). The model developed within this chapter aims to eliminate many of the assumptions made in the more simple rate equation models whilst holding on to its numerical attractiveness – a feature which is missing from many of the more advanced models. To this end, all key model parameters needed to model the heating of the degenerate gases in the QW will be calculated directly from the non-parabolic band structure and stored as a function of hole quasi-Fermi level, electron quasi-Fermi level, electron temperature and hole temperature. This eliminates many of the assumptions of the more simple models. The model parameters calculated from the non-parabolic band

structure include:

- Average electron energy
- Average hole energy
- Electron energy density
- Hole energy density
- Average energy of the electrons/holes involved in stimulated emission
- Average energy of the electrons/holes involved in spontaneous emission
- Gain
- Spontaneous emission

The calculation of these parameters is a computationally expensive process. Therefore, these values are tabulated prior to the simulation and stored in look-up tables ready for use at simulation time. This model is then used to investigate the impact of the LO-phonon bottleneck in the dilute nitride devices investigated in the previous chapters. Both the steady-state behaviour of the hot carrier populations and large-signal transient response are examined.

7.5 A numerical overview

The 2D electro-optical-thermal simulation tool presented in Chapter 5 is extended with a four-temperature energy balance model for each QW. This consists of energy balance equations for the electron (7.24), hole (7.26) and LO-phonon (7.31) energies. These equations are solved self-consistently with the other device equations to obtain the non-equilibrium LO-phonon (T_{LO}), electron (T_e), hole (T_h) and lattice (T_L)

temperatures. The 2D carriers in the QW are heated by carrier relaxation from the bulk states to the lasing states (H_{CAP}), free carrier absorption (H_{FCA}) and lateral joule heating (H_J). The QW carriers lose energy through the emission of photons via stimulated (R_{Stim}), spontaneous emission (R_{Spon}) recombination and via the emission of acoustic and LO-phonons.

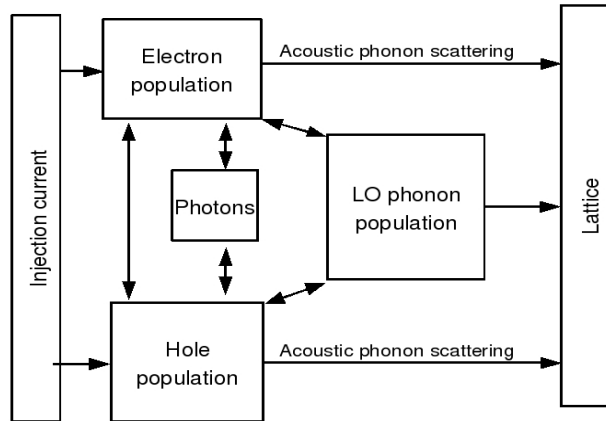


Figure 7.3: Schematic diagram of the energy pathways within the model.

The non-equilibrium LO-phonons have a finite lifetime (τ_{LO-a}) and decay into acoustic phonons. The scattering time τ_{LO-a} is calculated as a function of the lattice temperature using equation (7.45). The energy pathways of the model are shown in figure 7.3. The QW carrier energy densities ($U^{e/h}$), average lasing energy (\bar{E}^{stim}) and average spontaneous emission energy (\bar{E}^{spon}) required for this model are calculated from the non-parabolic band structure (7.3-7.5). Carrier-carrier scattering between the electron and hole populations is treated using the relaxation approximation with the scattering time constant.

The QW valance band structure is calculated using a 4x4 band **k.p** model and (for the dilute nitride materials) the conduction band using a band anti-crossing model. The non-parabolic band structure is used to calculate the carrier densities, gain and spontaneous emission rates as a function of the quasi-Fermi level position, electron temperature and hole temperature. In the following sections, the model will be described in more detail.

7.6 Preliminaries

Before the model can be described in detail, some preliminary definitions must be made.

7.6.1 Electron densities

The electron and hole densities in the QW are calculated using,

$$n(F_e, T_e) = \frac{1}{L_w} \sum_{i=0}^{N_e} \int_{E_i^0}^{\infty} D_i^e(E) f_e(E, F_e, T_e) dE \quad (7.1)$$

and

$$p(F_h, T_h) = \frac{1}{L_w} \sum_{i=0}^{N_v} \int_{E_i^0}^{\infty} D_i^h(E) f_h(E, F_h, T_h) dE \quad , \quad (7.2)$$

where $N_{e/h}$ is the number of conduction/valance bands in the QW and $D^{e/h}(E)$ is the 2D density of the electron states in the conduction/valance band. $D^{e/h}(E)$ is a numerical function calculated from the band structure. The total 2D carrier density is divided by L_w to give the QW carrier density in m^{-3} .

7.6.2 Carrier energy density

The carrier energy density is calculated in the same way, except that an energy term is included in the integral. Again, the expression is divided by the quantum well width to convert the 2D energy density into a 3D energy density resulting in

$$U_{e/h}(F_{e/h}, T_{e/h}) = \frac{\sum_{i=0}^N \int_0^{\infty} E D_i^{e/h}(E) f_{e/h}(E, F_{e/h}, T_{e/h}) dE}{L_w}. \quad (7.3)$$

7.6.3 Average carrier energy

To calculate the average carrier energy, equation 7.3 is divided by the 2D carrier density to give

$$\bar{E}^{e/h}(F_{e/h}, T_{e/h}) = \frac{\sum_{i=0}^N \int_0^{\infty} E D_i^{e/h}(E) f_{e/h}(E, F_{e/h}, T_{e/h}) dE}{\sum_{i=0}^N \int_0^{\infty} D_i^{e/h}(E) f_{e/h}(E, F_{e/h}, T_{e/h}) dE L_w}. \quad (7.4)$$

7.6.4 Average lasing energies

The average energy of the lasing electrons is calculated using

$$\bar{E}_{Stim}^{e/h}(T_e, T_h, n, p, \hbar\omega) = \frac{\int_0^{\infty} \sum_{i=0}^N R_{stim}^n(E, T_e, T_h, n, p) L(\hbar\omega - E) E dE}{\int_0^{\infty} \sum_{i=0}^N R_{stim}^n(E, T_e, T_h, n, p) L(\hbar\omega - E) dE}. \quad (7.5)$$

It is assumed that the laser has one mode which lases at the peak of the gain spectra. Equation 7.5, is therefore only evaluated at $\hbar\omega_{peak}$. The stimulated recombination rate is calculated through

$$R_{\text{stim}}^n(E, T_e, T_h, n, p) = \left(\frac{\Phi_{PHC}}{n \hbar \omega} \right) \frac{\pi e^2 \hbar}{\epsilon_0 c m_0^2 \bar{n}} |M_T|^2 \rho_{\text{red}}(E_{eh} - E'_g) (f_e(T_e) - f_h(T_h)) . \quad (7.6)$$

More details on the calculation of the gain are provided in Chapter 5.

7.6.5 Average carrier energies taking place in spontaneous emission

The average energy of a carrier taking part in spontaneous recombination is given as

$$\bar{E}_{elh}^{\text{spont}} = \frac{\int_0^\infty \sum_{i=0}^N R_{\text{spont}}(E, T_e, T_h) E dE}{\int_0^\infty \sum_{i=0}^N R_{\text{spont}}(E, T_e, T_h) dE} , \quad (7.7)$$

where the summation is over all sub band pairs.

7.6.6 Heat capacities

The heat capacity is defined as the change of the internal energy of a system with respect to temperature. For the electron gas, the heat capacity is given as

$$C_e(F_e, T_e) = \frac{1}{L_w} \sum_{i=0}^N \frac{\partial}{\partial T} \int_0^\infty E D_i^e(E) f_e(E, F_e, T_e) dE , \quad (7.8)$$

and for the hole gas it is given as

$$C_h(F_h, T_h) = \frac{1}{L_w} \sum_{i=0}^N \frac{\partial}{\partial T} \int_0^\infty E D_i^h(E) f_h(E, F_h, T_h) dE . \quad (7.9)$$

7.6.7 The effective band gap

In the following work, it is useful to define the average energy separation of the

electron and hole populations. This will be referred to as the *average electron/hole energy difference* $\hat{E}_g^{qw}(T)$, and is given by the band gap energy of the QW plus the average electron and hole energies,

$$\hat{E}_g^{qw}(T) = E_g + \bar{E}^e(T_e, F_e) + \bar{E}^h(T_h, F_h) . \quad (7.10)$$

The last two terms in equation 7.10 are calculated from equation 7.7.

7.7 Electron/hole rate equations

The fundamental rate equation describing the conservation of carrier energy is

$$\left\langle \frac{\partial U}{\partial t} \right\rangle = \left\langle \frac{\partial U}{\partial t} \right\rangle_{FCA} + \left\langle \frac{\partial U}{\partial t} \right\rangle_{inj} - \left\langle \frac{\partial U}{\partial t} \right\rangle_{Recomb} - \left\langle \frac{\partial U}{\partial t} \right\rangle_{Spont} - \left\langle \frac{\partial U}{\partial t} \right\rangle_{Stim} - \left\langle \frac{\partial U}{\partial t} \right\rangle_{c \rightarrow LO} - \left\langle \frac{\partial U}{\partial t} \right\rangle_{c \rightarrow AC} , \quad (7.11)$$

where U is the energy density of the carrier gas (Jm^{-3}). This equation states that carrier energy is conserved. Energy is gained via FCA, carrier injection and lost via radiative recombination, and relaxation via phonon emission. It is assumed that all heating events occur upon the carrier gas and that the gas thermalises instantaneously. The differentials are described in more detail table 7.1.

$\langle \partial U / \partial t \rangle$	Change of total energy density with time.
$\langle \partial U / \partial t \rangle_{FCA}$	Increase in energy density due to free carrier absorption heating.
$\langle \partial U / \partial t \rangle_{inj}$	Energy gain via electron injection from bulk.
$\langle \partial U / \partial t \rangle_{Recomb}$	Recombination heating.
$\langle \partial U / \partial t \rangle_{Spont}$	Spontaneous emission cooling.
$\langle \partial U / \partial t \rangle_{Stim}$	Stimulated emission cooling.
$\langle \partial U / \partial t \rangle_{e \rightarrow AC}$	Cooling of the electron gas to the LO phonon population.
$\langle \partial U / \partial t \rangle_{e \rightarrow LO}$	Cooling of the electron gas to the lattice temperature via acoustic phonon emission.

Table 7.1: Summary of cooling/heating terms.

7.8 Heating and cooling mechanisms

7.8.1 Heat capacity

If equation 7.11 is solved in steady state, there is no net change of energy.

Consequently,

$$\left\langle \frac{\partial U}{\partial t} \right\rangle = 0 . \quad (7.12)$$

However, if the simulation is to be solved in the time domain, the total change of energy density is non-zero. The expression for change of carrier energy density with time can be directly solved

$$\left\langle \frac{\partial U_{e/h}}{\partial t} \right\rangle = \frac{U_t - U_{t-1}}{\partial t} , \quad (7.13)$$

where U_{t-1} is the energy density of the previous time step and U_t is the energy density

at the current time step. The energy density can be evaluated using 7.3.

7.8.2 Free carrier absorption

Free carrier absorption heating acts directly on the confined carrier gases. For electrons, FCA heating is given as

$$\left\langle \frac{\partial U}{\partial t} \right\rangle_{\text{FCA}}^e = \alpha_n^0 n_{qw} \Phi_{PH} \hbar \omega \quad (7.14)$$

and for holes it is given as

$$\left\langle \frac{\partial U}{\partial t} \right\rangle_{\text{FCA}}^h = \alpha_p^0 p_{qw} \Phi_{PH} \hbar \omega \quad (7.15)$$

More detail on FCA can be found in Chapter 5.

7.8.3 Energy loss via stimulated emission

As carriers radiately recombine, energy is lost from the carrier populations. This is modelled using,

$$\left\langle \frac{\partial U}{\partial t} \right\rangle_{\text{Spont}}^e + \left\langle \frac{\partial U}{\partial t} \right\rangle_{\text{Stim}}^e = \bar{E}_{\text{Spont}}^e(T) R_{\text{Spont}} + \bar{E}_{\text{Stim}}^e(T) R_{\text{Stim}} \quad (7.16)$$

for the electron population and

$$\left\langle \frac{\partial U}{\partial t} \right\rangle_{\text{Spont}}^h + \left\langle \frac{\partial U}{\partial t} \right\rangle_{\text{Stim}}^h = \bar{E}_{\text{Spont}}^h(T) R_{\text{Spont}} + \bar{E}_{\text{Stim}}^h(T) R_{\text{Stim}} \quad (7.17)$$

for the hole population, where R_{spont} and R_{stim} are the spontaneous and the stimulated recombination rates, respectively. These are calculated from the non-parabolic band structure. $\bar{E}_{\text{Spont}}^{e/h}(T)$ and $\bar{E}_{\text{Stim}}^{e/h}(T)$ are average energies of the carriers participating

in stimulated and spontaneous emission recombination. Note that this energy is substantially below that of the average QW carrier energy, so that the average energy of the remaining carriers increases.

7.8.4 Optical phonon emission

As previously discussed, LO-phonon scattering is the dominant carrier relaxation mechanism in GaInAsN quantum wells (this is also true for GaInAs QWs). This is modelled as an energy rate equation

$$\left\langle \frac{\partial U}{\partial t} \right\rangle_{e/h \rightarrow LO} = \left(\frac{U^{e/h}(T_{e/h}) - U^{e/h}(T_{LO})}{\tau_{LO-e/h}} \right), \quad (7.18)$$

which describes the carrier gases relaxing towards the hot LO-phonon temperature T_{LO} , where $\tau_{LO-e/h}$ is the scattering time.

7.8.5 Acoustic phonon emission

Although LO-phonon emission is the dominant cooling mechanism, the carriers also decay (to a much lesser extent) via acoustic phonon emission. This is taken into account using the following rate equation

$$\left\langle \frac{\partial U}{\partial t} \right\rangle_{e/h \rightarrow AC} = \left(\frac{U_{ke}^{e/h \text{ den}}(T_{e/h}) - U_{ke}^{e/h \text{ den}}(T_L)}{\tau_{AC-e/h}} \right). \quad (7.19)$$

where $U_{ke}^{e/h \text{ den}}(T_{e/h})$ is the energy density of the electron gas at the elevated temperature $T_{e/h}$ and $U_{ke}^{e/h \text{ den}}(T_L)$ is what the energy density the electron gas would be if it were at the lattice temperature. The time constant $\tau_{AC-e/h}$ is the carrier/acoustic

phonon scattering time.

7.8.6 Shockley-Read-Hall recombination

In Shockley-Read-Hall (SRH) recombination, an electron and hole recombine through a deep-level on a lattice defect state. This state is usually taken as being midway between the conduction and valance band edges. Both the electron and hole populations lose a carrier via this process. The energy lost can be assumed to be transferred straight to the lattice as heat. Therefore, SRH has a heating effect on the lattice and removes energy from the carrier gases. The heating effect on the lattice is modeled as the rate of SRH recombination multiplied by the average electron/hole energy difference (The QW band gap plus the average carrier energy of the electrons and holes is defined earlier)

$$H_{1\text{SRH}} = R_{\text{SRH}} \widehat{E}_g^{qw}(T_L) . \quad (7.20)$$

The electron/hole gases lose energy equal to the average energy of an electron/hole multiplied by the rate of emission and is given by

$$H_{\text{SRH}}^{e/h} = -\frac{1}{2} R_{\text{SRH}} \overline{E}^{e/h}(T_L) . \quad (7.21)$$

7.8.7 Auger recombination in the QW

In Auger recombination, an electron/hole pair recombines and the energy is transferred to another electron/hole. This electron/hole then relaxes emitting phonons. The laser simulator only has one Auger scattering rate. It is therefore assumed that

half of the Auger scattering events originate in the electron population and the other half in the hole population. When the scattering event occurs, the energy lost to each carrier gas due to recombination is given as $-1/2 R_{aug} \bar{E}^{e/h}$. It is assumed that the excited carrier scatters up out of the QW back into the bulk and does not re-enter the QW. Thus, the total heating of the carrier populations due to Auger recombination is given by

$$H_{Auger}^{e/h} = -\frac{1}{2} R_{aug} \bar{E}^{e/h} . \quad (7.22)$$

The excited carrier which has been ejected from the QW is then assumed to relax in the bulk to the bottom of the band edge. Thus the heat H_{bulk} is given to the lattice

$$H_{bulk} = R_{SRH} \left(\widehat{E}_g^{qw} - \Delta E_{c/v} \right) , \quad (7.23)$$

where $\Delta E_{c/v}$ is energy difference between the average carrier energy in the conduction or valance band and the bulk band edge.

7.8.8 Final electron/hole rate equations

Placing all the above heat sources and relaxation time approximations into 7.11 results in

$$\begin{aligned} \frac{dU_e}{dt} = & \frac{H_{cap}^e + H_{SRH}^e + H_{Auger}^e +}{H_J^e - \bar{E}_{Stim}^e(T) R_{stim} - \bar{E}_{spon}^e(T) R_{spon} -} \\ & \frac{U_e(T_e) - U_e(T_{LO})}{\tau_{LO-e}} - \frac{U_e(T_e) - U_e(T_L)}{\tau_{AC-e}} . \quad (7.24) \\ & - \frac{U^e(T_e) - U^e(T_h)}{\tau_{eh}} + \frac{U^h(T_h) - U^h(T_e)}{\tau_{eh}} \end{aligned}$$

This equation is a *highly* non linear integro-differential equation, where the energy densities and average energy densities are all integrals (described above). The most efficient way of solving such an equation is Newton's method. In order to use Newton's method, the equation must be written as an error function. In this chapter, e will be used to denote the error. Thus equation 7.24 can be rewritten as

$$\begin{aligned}
e_e(T_e, T_h, T_L, T_{LO}) = & -\frac{dU_e}{dt} + H_{cap}^e + H_{SRH}^e + H_{Auger}^e + \\
& \frac{H_J^e - \bar{E}_{Stim}^e(T) R_{stim} - \bar{E}_{spon}^e(T) R_{spon} -}{U_e(T_e) - U_e(T_{LO})} - \frac{U_e(T_e) - U_e(T_L)}{U_e(T_e) - U_e(T_L)} \\
& - \frac{U^e(T_e) - U^e(T_h)}{\tau_{LO-e}} + \frac{U^h(T_h) - U^h(T_e)}{\tau_{AC-e}} \\
& - \frac{U^e(T_e) - U^e(T_h)}{\tau_{eh}} + \frac{U^h(T_h) - U^h(T_e)}{\tau_{eh}}
\end{aligned} \tag{7.25}$$

for the electron population and

$$\begin{aligned}
e_h(T_e, T_h, T_L, T_{LO}) = & -\frac{dU_h}{dt} + H_{fca}^h + H_{SRH}^h + H_{Auger}^h \\
& - \frac{\bar{E}_{Stim}^h(T) R_{Spon} + \bar{E}_{Spon}^h(T) R_{Stim}}{U^h(T_h) - U^h(T_{LO})} - \frac{U^h(T_h) - U^h(T_L)}{U^h(T_h) - U^h(T_L)} \\
& + \frac{U^e(T_e) - U^e(T_h)}{\tau_{LO-h}} - \frac{U^h(T_h) - U^h(T_e)}{\tau_{AC-h}} \\
& + \frac{U^e(T_e) - U^e(T_h)}{\tau_{eh}} - \frac{U^h(T_h) - U^h(T_e)}{\tau_{eh}}
\end{aligned} \tag{7.26}$$

for the hole population.

7.9 The hot LO-phonon population

7.9.1 The LO-phonon rate equation

As the carriers relax from the bulk states to the confined lasing states, LO-phonons are emitted. The rate equation describing the conservation of energy for the LO-phonon population is given by

$$\left\langle \frac{\partial U_{LO}}{\partial t} \right\rangle = \left\langle \frac{\partial U}{\partial t} \right\rangle_{e \rightarrow LO} + \left\langle \frac{\partial U}{\partial t} \right\rangle_{h \rightarrow LO} - \left\langle \frac{\partial U_{LO}}{\partial t} \right\rangle_{ac} . \quad (7.27)$$

The components of this equation are given in table 7.2.

$\left\langle \frac{\partial U_{LO}}{\partial t} \right\rangle$	Net change of energy of the LO-phonon population.
$\left\langle \frac{\partial U}{\partial t} \right\rangle_{e \rightarrow LO}$	Heating of the LO-phonon population by the electron relaxation (see section 7.8.4).
$\left\langle \frac{\partial U}{\partial t} \right\rangle_{h \rightarrow LO}$	Heating of the LO-phonon population by the hole relaxation (see section 7.8.4).
$\left\langle \frac{\partial U_{LO}}{\partial t} \right\rangle_{ac}$	Cooling of the LO-phonon population by the decay of LO-phonons into acoustic phonons.

Table 7.2: Summary of cooling/heating terms for the LO-phonon gas.

The rate of decay of optical phonons is described by

$$\left\langle \frac{\partial U_{LO}}{\partial t} \right\rangle_{ac} = \frac{U_{LO}(T_{LO}) - U_{LO}(T_L)}{\tau_{LO-a}} , \quad (7.28)$$

where $U_{LO}(T_{LO})$ is the energy density of the non-equilibrium LO-phonon population at temperature T_{LO} , i.e. the elevated temperature. $U_{LO}(T_L)$, is the energy density of the hot phonon population when relaxed to the lattice temperature. In steady state, the net change of energy is zero. Thus, the left hand side of equation 7.27 can be set to zero

$$\left\langle \frac{\partial U_{LO}}{\partial t} \right\rangle = 0 . \quad (7.29)$$

When a time domain solution is required, a finite difference scheme in the time domain is applied

$$\left\langle \frac{\partial U_{LO}}{\partial t} \right\rangle = \frac{U_t - U_{t-1}}{\Delta t} , \quad (7.30)$$

where U_t is the current LO-phonon density and U_{t-1} is the LO-phonon energy density Δt seconds ago. Writing the rate equation out in full gives

$$e_{LO}(T_e, T_h, T_L, T_{LO}) = -\frac{U_t^{LO} - U_{t-1}^{LO}}{\Delta t} + \frac{U^e(T_e) - U^e(T_{LO})}{\tau_{LO-e}} + \frac{U^h(T_h) - U^h(T_{LO})}{\tau_{LO-h}} - \frac{U_{LO}(T_{LO}) - U_{LO}(T_L)}{\tau_{LO-a}} . \quad (7.31)$$

7.9.2 The hot phonon energy density

The hot phonon energy density, U_{LO} , is one of the most critical components of the model. In the past, *Einstein's model* for heat capacity has been used to calculate U_{LO} . This assumes a quasi-equilibrium situation, where hot phonons occupy the entire 3D k-space density of phonon states. *Einstein's model* assumes N independent harmonic oscillators, each oscillating at the LO-phonon frequency. This model gives the energy density as

$$U_{LO} = \frac{3N \hbar \omega}{V_{qw}} \left(\frac{1}{2} + \frac{1}{e^{\hbar \omega / k T_{LO}} - 1} \right) , \quad (7.32)$$

where V_{qw} is the volume of the quantum well. However, the 2D confined carriers do not interact with the entire 3D LO-phonon k-space. The carriers exist within a continuum of k_{xy} momentum and have discretised k_z vectors. This imposes two limits

on the carrier/phonon interaction. Firstly, the maximum k_{xy} vector that can be generated via intraband scattering is limited by the maximum LO-phonon energy and the width in k-space of the top of the band. This is depicted in figure 7.4, where a carrier at the top of the band loses the maximum possible amount of xy-momentum to a phonon by relaxing from the maximum positive k_{xy} -vector to the smallest negative k_{xy} -vector. Assuming parabolic bands, Δk_{xy} is given by,

$$\Delta k_{xy}^{max} = \sqrt{\frac{2m \Delta E_b}{\hbar^2}} + \sqrt{\frac{2m (\Delta E_b - E_{LO})}{\hbar^2}}, \quad (7.33)$$

where ΔE_b is the difference in terms of energy between the top of the band and the bottom (see figure 7.4).

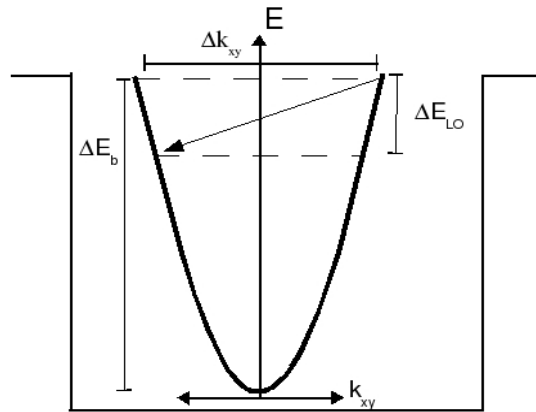


Figure 7.4: Maximum k_{xy} vector generated by an intraband carrier relaxation.

There is also a minimum limit to the generation of phonons via intraband relaxation. The dispersion curve for LO-phonons is flat - a carrier under 32meV in the band can not lose energy via LO-phonon emission. This is depicted in figure 7.5 and described analytically for parabolic bands as

$$\Delta k_{xy}^{min} = \sqrt{\frac{2m E_{LO}}{\hbar^2}} . \quad (7.34)$$

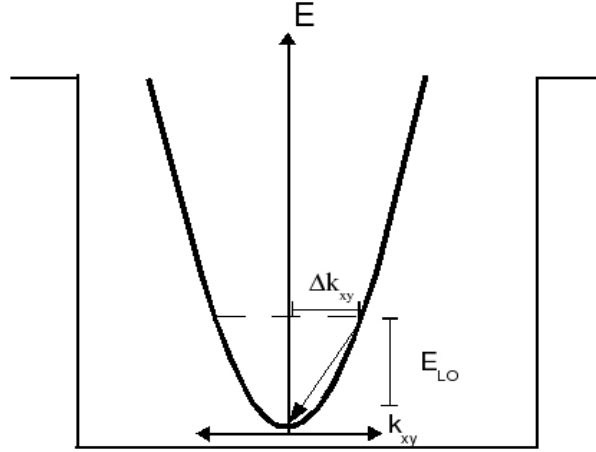


Figure 7.5: Minimum excited k_{xy} vector due to carrier/LO-phonon interaction.

The second restriction on carrier/LO-phonon interaction is that each band in the QW exists at a different discrete k_z wavevector (i.e. momentum is quantised normal to the plane.) Assuming that momentum is completely conserved normal to the plane, this means that only LO-phonons with k_z equal to the difference between the k_z momentum of the two bands will be generated. i.e.

$$k_z^{LO} = k_z^{\text{band 1}} - k_z^{\text{band 2}} . \quad (7.35)$$

Intraband LO-phonon scattering is, however, an order of magnitude faster than interband scattering [9]. Thus, far more LO-phonons with $k_z=0$ will be produced than $k_z \neq 0$. Thus, when calculating the energy density of the hot LO-phonon population,

one should consider a 2D flat disk rather than a 3D ball in k-space. Normally, that would be the end of the story. However, in narrow wells, momentum is apparently not conserved normal to the QW [10]. This is because of the uncertainty principle,

$$(\Delta x)(\Delta p_x) \geq \frac{\hbar}{2}. \quad (7.36)$$

As the quantum well is narrowed (<35nm for GaInAs), the position of the carriers become better defined, this means that the momentum becomes less well defined, thus transitions can occur where momentum is not conserved. The matrix element used to calculate the transition probability is multiplied by

$$|F(q_z)|^2 = \left| \int_0^w dz \psi_m^*(z) \psi_n(z) \exp(iq_z z) \right|^2, \quad (7.37)$$

which accounts for this blurring of the interacting states [11]. The result is a blurring of the 2D flat disk into a 3D doughnut shape. The k-vectors partaking in the transitions can be approximated by

$$\frac{q_z}{2} = \frac{2\pi}{L_w}, \quad (7.38)$$

where L_w is the QW width [11]. The energy density of the non-equilibrium LO-phonons can now be calculated by integrating over the volume of k-space they occupy, multiplied by the density and the Bose-Einstein occupational probability,

$$U_{\text{LO}}(T) = \frac{\hbar \omega_{\text{LO}}}{(2\pi)^3} \int_{q_{xy}^{\min}}^{q_{xy}^{\max}} \int_0^{2\pi} N(T) d\theta dk_{xy} \int_{-\delta q_z/2}^{\delta q_z/2} dq_z \quad (7.39)$$

where $N(T)$ is the Bose-Einstein occupation probability given by,

$$N(T) = \frac{1}{e^{\hbar \omega_{LO}/kT} - 1}, \quad (7.40)$$

and where δq is the width of the disk, θ sweeps out the angle of integration, q_{\min} and q_{\max} are the maximum and minimum vectors of for k_{xy} . The equation

$$N_s = \frac{V_k}{(2\pi/L)^m} \quad (7.41)$$

with $m=3$ has been used to calculate the density of states. Evaluating equation 7.39 by integrating θ between 0 and 2π gives

$$U_{LO}(T) = \frac{\hbar \omega_{LO}}{(2\pi)^2} \int_{d_{xy}^{\min}}^{d_{xy}^{\max}} k_{xy} N(T) dk_{xy} \int_{-\delta q_z/2}^{\delta q_z/2} dq_z. \quad (7.42)$$

At the beginning of a simulation, equation 7.42 is solved numerically from 250K to 500K in 0.05K steps, and the results are stored in a look up table. This eliminates the need for a slow numerical evaluation of the integral during the simulation.

7.9.3 Lattice heat flux

The final part of the model is to describe the heat propagating out of the device. The lattice heat flux equation as described in Chapter 5 is written again in equation 7.43. This time, however, the heating terms associated with the QW have been replaced by energy relaxation approximations. The third term from the left in equation 7.43 describes the heating due to LO-phonon decay from the hot LO-phonon gas. The last two terms describe the energy transferred to the lattice via carrier relaxation via acoustic phonons,

$$C_L \frac{\partial T_L}{\partial t} = \nabla k_L \nabla T + H_{\text{bulk}} + \frac{U^{\text{LO}}(T_{\text{LO}}) - U^{\text{LO}}(T_L)}{\tau_{\text{LO}-a}} + \frac{U^e(T_e) - U^e(T_L)}{\tau_{\text{AC}-e}} + \frac{U^h(T_h) - U^h(T_L)}{\tau_{\text{AC}-h}}. \quad (7.43)$$

Equation 7.43 is then rearranged in terms of an error function ready to be solved by Newton's method,

$$e_L(T_e, T_h, T_L, T_{\text{LO}}) = -C_L \frac{T_L^i - T_L^{i-1}}{\Delta t} + \nabla k_L \nabla T + H_{\text{bulk}} + \frac{U^{\text{LO}}(T_{\text{LO}}) - U^{\text{LO}}(T_L)}{\tau_{\text{LO}-a}} + \frac{U^e(T_e) - U^e(T_L)}{\tau_{\text{AC}-e}} + \frac{U^h(T_h) - U^h(T_L)}{\tau_{\text{AC}-h}}. \quad (7.44)$$

7.10 Relaxation times used

The relaxation times used in the simulation are given below in table 7.3.

<i>Event</i>	<i>Time</i>	<i>Reference</i>
$\tau_{\text{e-h}}$	1ps	[12]
$\tau_{\text{LO}}^{\square}$	8ps	[13]
$\tau_{\text{AC-e}}$	1ns	[14]
$\tau_{\text{AC-h}}$	0.5ns	[14]
$\tau_{\text{LO-e}}$	142fs	[15]
$\tau_{\text{LO-h}}$	71fs	[15]

Table 7.3: Scattering times used

The LO-phonon relaxation time is given as a function of lattice temperature. This dependence is given as

$$\tau_{\text{LO}-a} = \frac{\tau_{\text{LO}}^0}{1 + 2 \left[\exp(0.5 \hbar \omega_{\text{LO}}) / k_B T_L - 1 \right]^{-1}}. \quad (7.45)$$

7.11 A simplified model

In the literature, more simplified models are often used, where it is assumed that the carriers in the quantum well have a kinetic energy of kT . i.e. they are treated as a 2D gas and from partition theory, each dimension gives $1/2kT$ worth of energy. It is also commonly assumed that all recombination (dark and radiative) occurs at kT from the bottom of the band. The main advantage of this approach is the simplicity of the model and its good numerical stability. In order to compare the more accurate simulation performed here with these models, an option to turn on this simplified model was included. The simplified set of definitions is

$$U_e(T) = kT_e n, \quad (7.46)$$

$$U_h(T) = kT_h p, \quad (7.47)$$

$$\bar{E}^{e/h}(T) = kT_{e/h}, \quad (7.48)$$

$$\bar{E}_{Stim}^{e/h}(T_e, T_h, n, p, \hbar\omega) = kT_{e/h}, \quad (7.49)$$

$$E_{spon}^{e/h} = kT_{e/h} \text{ and} \quad (7.50)$$

$$C_{e/h}(T) = k. \quad (7.51)$$

7.12 Solution of the problem

The set of equations given in sections 7.6-7.10 are a set of highly non-linear integro-differential equations. The most straight forward method of solution, for such a problem is Newton's method, as described in Chapter 5. The 1D problem is of the form (7.52).

$$\begin{bmatrix} \frac{\partial e_L}{\partial T_L} & \frac{\partial e_L}{\partial T_e} & \frac{\partial e_L}{\partial T_h} & \frac{\partial e_L}{\partial T_{LO}} \\ \frac{\partial e_e}{\partial T_L} & \frac{\partial e_e}{\partial T_e} & \frac{\partial e_e}{\partial T_h} & \frac{\partial e_e}{\partial T_{LO}} \\ \frac{\partial e_h}{\partial T_L} & \frac{\partial e_h}{\partial T_e} & \frac{\partial e_h}{\partial T_h} & \frac{\partial e_h}{\partial T_{LO}} \\ \frac{\partial e_{LO}}{\partial T_L} & \frac{\partial e_{LO}}{\partial T_e} & \frac{\partial e_{LO}}{\partial T_h} & \frac{\partial e_{LO}}{\partial T_{LO}} \end{bmatrix} \begin{bmatrix} \Delta T_L \\ \Delta T_e \\ \Delta T_h \\ \Delta T_{LO} \end{bmatrix} = - \begin{bmatrix} e_L \\ e_e \\ e_h \\ e_{LO} \end{bmatrix} \quad (7.52)$$

One of the most efficient ways to solve the problem is a sparse matrix LU decomposition algorithm. The algorithms `f01brf()` and `f04axf()` from the Numerical Algorithms Group (NAG) were used. `F01brf()` is a sparse matrix factorisation routine, which is used to separate the Jacobian into an upper and lower part. `f04axf()` is used to solve for the update $\Delta T_{L,e,h,LO}$

$$T_L^{k+1} = T_L^k + \Delta T_L^{k+1} \quad , \quad (\text{Error: Reference source not found 7.53})$$

$$T_e^{k+1} = T_e^k + \Delta T_e^{k+1} \quad , \quad (7.54)$$

$$T_h^{k+1} = T_h^k + \Delta T_h^{k+1} \quad , \quad (7.55)$$

$$T_{LO}^{k+1} = T_{LO}^k + \Delta T_{LO}^{k+1} \quad . \quad (7.56)$$

The QW is very small when compared to the rest of the epitaxial device structure. In terms of mesh points, around ten points are used to model the QW whereas around one to two hundred mesh points are used to model the much larger bulk. Thus, the matrix elements e_L representing the 1D heat equation (i.e. a bulk equation) far outnumber those representing the QW. The Jacobian is typically $\sim 200 \times 200$ in size,

$$\frac{\partial e_L}{\partial T_h} = \frac{1}{\tau_{AC-h}} \frac{\partial U_h(T_h)}{\partial T_h} \quad (7.61)$$

$$\frac{\partial e_L}{\partial T_{LO}} = \frac{1}{\tau_{LO-a}} \frac{\partial U_{LO}(T_{LO})}{\partial T_{LO}} \quad (7.62)$$

where $\frac{\partial}{\partial T_L}(\nabla k_L \nabla T)$ has been defined earlier.

7Error: Reference source not found.12.2 Electron energy conservation equation

$$\frac{\partial e_e}{\partial T_L} = \frac{1}{\tau_{AC-e}} \frac{\partial U_e(T_L)}{\partial T_L} \quad (7.63)$$

$$\begin{aligned} \frac{\partial e_e}{\partial T_e} = & -\frac{1}{\Delta t} \frac{U_e(T_e^t)}{\partial T_e} - \frac{1}{\tau_{LO-e}} \frac{\partial U_e(T_e)}{\partial T_e} - \\ & \frac{1}{\tau_{AC-e}} \frac{\partial U_e(T_e)}{\partial T_e} - \frac{1}{\tau_{eh}} \frac{\partial U_e(T_e)}{\partial T_e} - \frac{1}{\tau_{eh}} \frac{\partial U_h(T_e)}{\partial T_e} \end{aligned} \quad (7.64)$$

$$\frac{\partial e_e}{\partial T_h} = \frac{1}{\tau_{eh}} \frac{\partial U_e(T_h)}{\partial T_h} + \frac{1}{\tau_{eh}} \frac{U_h(T_h)}{\partial T_h} \quad (7.65)$$

$$\frac{\partial e_e}{\partial T_{LO}} = \frac{1}{\tau_{LO-e}} \frac{\partial U_e(T_{LO})}{\partial T_{LO}} \quad (7.66)$$

7Error: Reference source not found.12.3 Hole energy conservation equation

$$\frac{\partial e_h}{\partial T_L} = \frac{1}{\tau_{AC-h}} \frac{\partial U_h(T_L)}{\partial T_L} \quad (7.67)$$

$$\frac{\partial e_h}{\partial T_e} = \frac{1}{\tau_{eh}} \frac{U_e(T_e)}{\partial T_e} + \frac{1}{\tau_{eh}} \frac{U_h(T_e)}{\partial T_e} \quad (7.68)$$

$$\begin{aligned} \frac{\partial e_h}{\partial T_h} = & -\frac{1}{\Delta t} \frac{\partial U_h(T_h)}{\partial T_h} - \frac{1}{\tau_{LO-h}} \frac{\partial U_h(T_h)}{\partial T_h} - \frac{1}{\tau_{AC-h}} \frac{U_h(T_h)}{\partial T_h} \\ & - \frac{1}{\tau_{eh}} \frac{U_e(T_h)}{\partial T_h} - \frac{1}{\tau_{eh}} \frac{U_h(T_h)}{\partial T_h} \end{aligned} \quad (7.69)$$

$$\frac{\partial e_h}{\partial T_{LO}} = \frac{1}{\tau_{LO-h}} \frac{\partial U_h(T_{LO})}{\partial T_{LO}} \quad (7.70)$$

7Error: Reference source not found.12.4 LO-phonon energy conservation equation

$$\frac{\partial e_{LO}}{\partial T_L} = \frac{1}{\tau_{LO-a}} \frac{\partial U_{LO}(T_L)}{\partial T_L} \quad (7.71)$$

$$\frac{\partial e_{LO}}{\partial T_e} = \frac{1}{\tau_{LO-e}} \frac{\partial U_e(T_e)}{\partial T_e} \quad (7.72)$$

$$\frac{\partial e_{LO}}{\partial T_h} = \frac{1}{\tau_{LO-h}} \frac{\partial U_h(T_h)}{\partial T_h} \quad (7.73)$$

$$\begin{aligned} \frac{\partial e_{LO}}{\partial T_{LO}} = & -\frac{1}{\Delta t} \frac{U_{LO}(T_{LO})}{\partial T_{LO}} - \frac{1}{\tau_{LO-e}} \frac{\partial U_e(T_{LO})}{\partial T_{LO}} \\ & - \frac{1}{\tau_{LO-h}} \frac{\partial U_h(T_{LO})}{\partial T_{LO}} - \frac{1}{\tau_{LO-a}} \frac{\partial U_{LO}(T_{LO})}{\partial T_{LO}} \end{aligned} \quad (7.74)$$

7Error: Reference source not found.12.5 Evaluation of the derivatives

The derivatives of the energy density for the carrier populations are numerically evaluated from tabulated solutions of 7.3, stored as a function of n , p , T_e and T_h . The derivatives of the LO-phonon energy density are also evaluated numerically from the tabulated solution. When using the simplified solution (equations 7.46 - 7.51), the derivatives are evaluated analytically.

7.13 The 1.3 μm dilute nitride device

This section investigates the impact of the non-equilibrium phonon population on the operation of the 1.3 μm lasers described earlier in this work.

7.13.1 The structure

The epitaxy of the 1.3 μm lasers simulated here is the same as those described in section 3.2. The device is 300 μm long, with uncoated facets ($R=0.32$) and a ridge waveguide (RW) width of 3.2 μm . A 100 μm wide thermal simulation window was used to simulate this device. The device is depicted in figure 7.6.

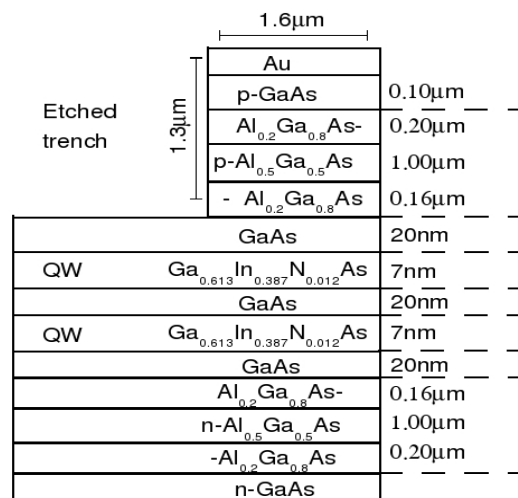


Figure 7.6: Laser epitaxial structure and etching profile.

7.13.2 Simulation results for the low power 1.3 μm device – Steady state

In figure 7.7, simulated LI-curves are plotted with and without the inclusion of the hot-phonon model. Below threshold, there is no impact on the LI curves, whilst at moderate injection levels, the predicted output decreases by $\sim 1\text{mW}$. At high injection currents, the inclusion of the hot phonon model decreases the predicted output power by up to 4mW . A super linear divergence of the two predicted output powers is observed. This indicates that importance of including the hot-phonon model becomes more important the harder a device is driven.

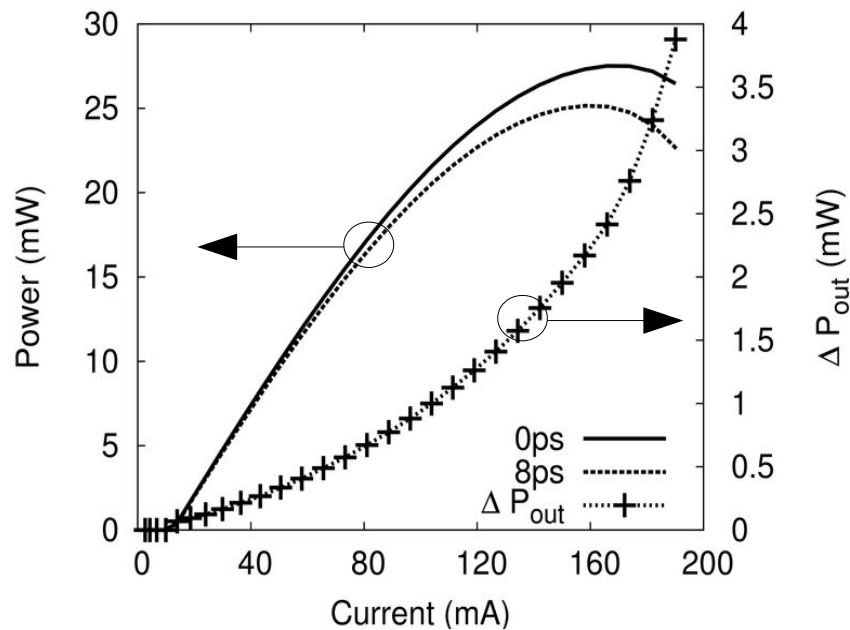


Figure 7.7: Light-current curves generated when the hot phonon model is included (8ps) and when it is not (0ps).

In figure 7.8, the quantum well temperatures corresponding to an LO-phonon relaxation time of 8ps are plotted as a function of injection current. The hot-phonon population is $\sim 10\text{K}$ above that of the lattice temperature. This temperature difference

increases as the injection current is increased. The carrier temperatures can be seen to 'ride' on the LO-phonon temperature. This is an expected result because the hot LO-phonon population also passes energy pack to the electron and hole gases through phonon absorption scattering processes.

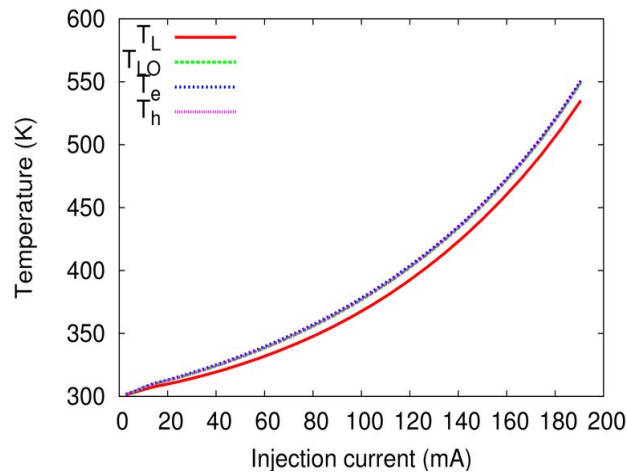


Figure 7.8: QW temperatures plotted against injection current for an 8ps scattering time.

Figure 7.9 plots the temperature difference between the hot LO-phonon temperature and the lattice temperature for a range of LO-phonon relaxation times. For a scattering time of 10ps, a >18K rise in the LO-phonon temperature relative to the lattice temperature is observed.

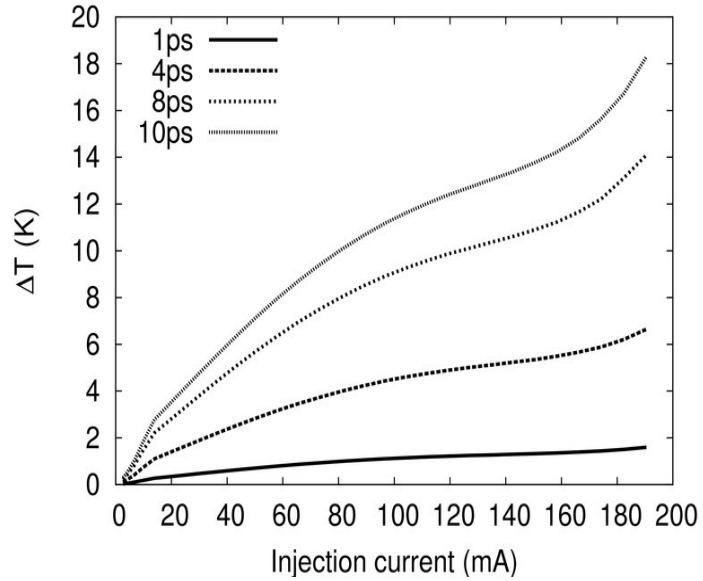


Figure 7.9: LO-phonon bottleneck temperature.

As the injection current is increased, the temperature difference between the carriers and the hot phonon population increases slowly. This is because as the injection current is increased and the device slowly heats. This reduces the optical gain, thus one of the QW carrier cooling mechanisms becomes less efficient, and the carriers heat up relative to the LO-phonon population.

Figure 7.10 shows, a thermal profile in the QW across the facet of the device when it is emitting 12mW of output power from the front facet. The centre of the ridge is at 0mm and the ridge extends to ± 1.6 mm, where the etch trench begins. The electron, hole, non-equilibrium LO-phonon and lattice temperatures are plotted. The temperature of the hot-phonon population under the ridge is ~ 7 K higher than that of the lattice. The elevated LO-phonon temperature corresponds to a high carrier injection rate, which generates a large number of LO-phonons. The carrier temperatures are only a couple of degrees above the LO-phonon temperature. The

electron population is hotter than the hole population, for two reasons. Firstly, the hole/LO-phonon scattering time (71fs) is far faster than the electron/LO-phonon scattering time (142fs), thus the hole population releases its energy to the hot LO-phonon population faster than the electron population does. Secondly, the conduction band QW is deeper than the valance band QW, so electrons have further to relax from the bulk states releasing more energy into the electron population than the hole population. Further away from the ridge, where the injection current is less, the populations approach a quasi-equilibrium distribution.

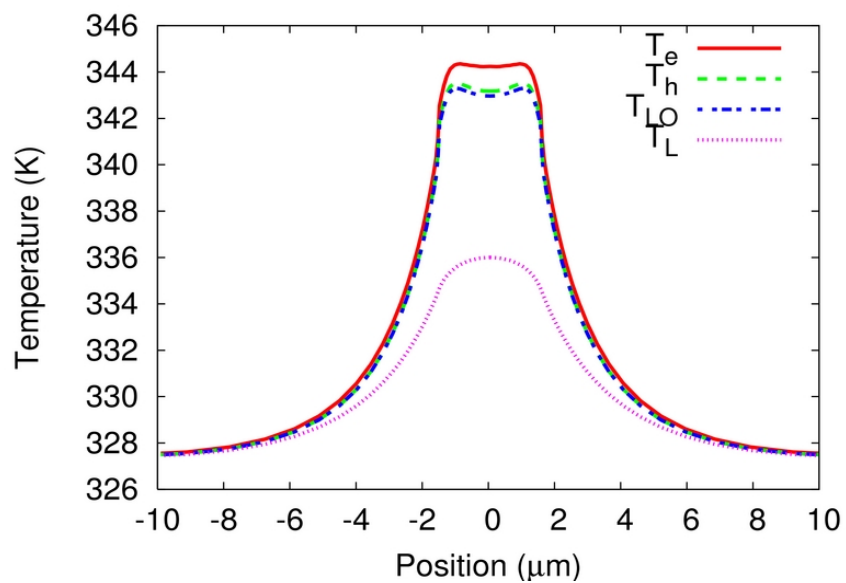


Figure 7.10: 2D temperature profile across the QW. The centre of the RW is at $0 \mu\text{m}$ as this is a half space simulation. ($T_{\text{Heatsink}} = 300 \text{ K}$.)

A typical 2D thermal profile is shown in figure 7.11. The region of high temperature at the top of the device is the ridge. The large flat area of low temperature at the lower end of the graph represents the substrate, whilst the QWs lie directly under the

ridge, represented by the black line. The lattice temperature profile in figure 7.10 corresponds to the temperature profile along the black line in figure 7.11.

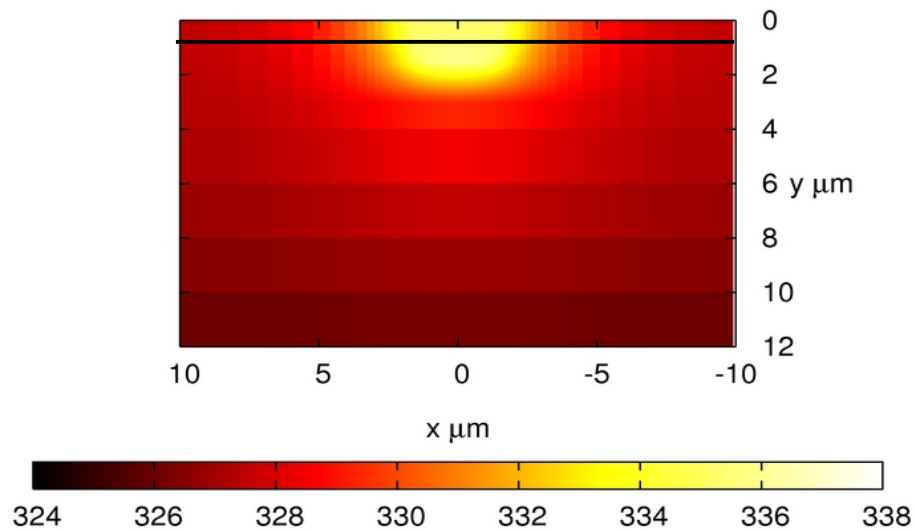


Figure 7.11: The 2D thermal profile of the device simulated with a front facet output power of 12mW. The black line represents the position of the QWs.

Figure 7.12, plots the temperature difference between the hot LO-phonon and the lattice temperature ($T_{LO}-T_L$) as a function of optical output power for different external heatsink temperatures. A super-linear increase in the temperature can be seen at heatsink temperatures above 360K, which is caused by the more constricted LO-phonon bottleneck. At lower heatsink temperatures (300-360 K), this behaviour is not observed because the LO-phonon decay time is shorter at lower temperatures (see equation 7.45). A high lattice temperature increases the carrier temperature, which in

turn reduces the optical gain due to thermal broadening of the carrier distributions. Therefore, to achieve the same optical output power at a higher heat sink temperature, a higher carrier density is required. This implies a larger injection current. When pumping the device harder, the LO-phonon bottleneck becomes more severe. Experimentally, the device shows a decrease in performance for heatsink temperatures above 360K, which is in part due to the more restrictive LO-phonon bottleneck.

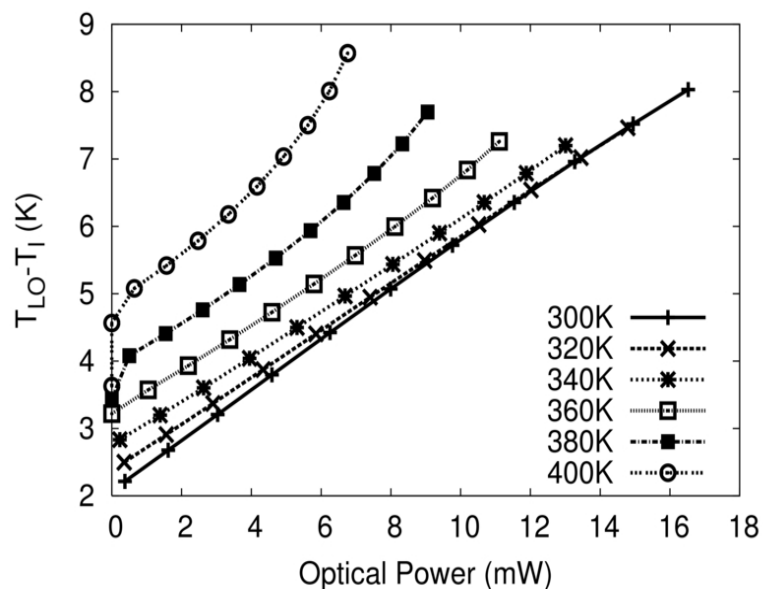


Figure 7.12: Phonon bottleneck as a function of front facet output power for varying heat sink temperatures.

7.13.3 Simulation results for the low power 1.3 μm device – Time domain

The optical output power from a 1D time domain simulation is shown in figure 7.13 for a bit rate of 10Gb/s . Simulations with and without the hot phonon model are shown. The impact of including the non-equilibrium LO-phonons is to reduce the peak optical power by up to 2mW. Again, this is due to the elevated carrier

temperatures, which reduce the optical gain. The pulse is also delayed and the rise in the optical power slower when the hot-phonon model is included.

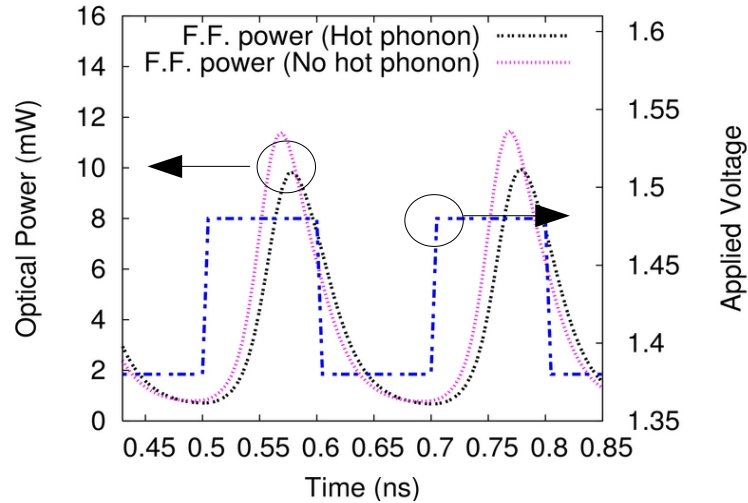


Figure 7.13: Time domain response of optical output power to applied voltage pulse train. ($T_{\text{Heatsink}} = 300 \text{ K}$), $T_L = 339 \text{ K}$.

The non-equilibrium QW temperatures for this example are plotted in figure 7.14. The hot LO-phonon temperature is seen to increase by up to 3K within the width of the modulating pulse. The carrier temperatures are seen to follow the hot LO-phonon temperature throughout the pulse train, this is because of the short e-LO and h-LO scattering times.

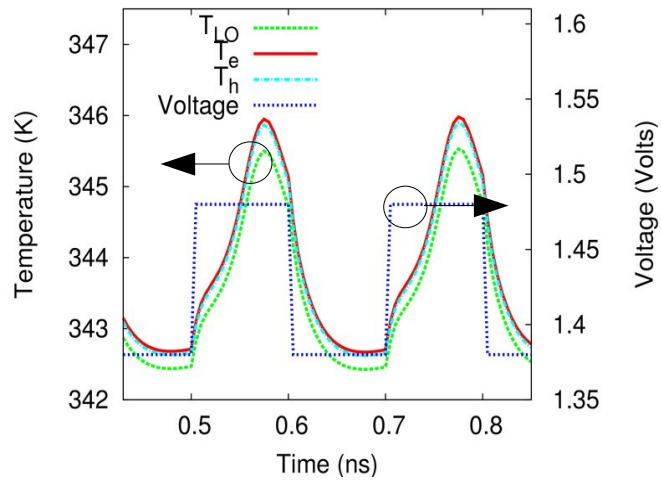


Figure 7.14: Time domain response of T_{LO} , T_e , T_h to applied voltage pulse train. ($T_{Heatsink} = 300$ K, $T_L = 339$ K.)

The LO-phonon temperature for each QW is plotted in figure 7.15. The temperatures are very slightly different due to the slightly different positions within the epitaxy. QW1 is closer to the ridge i.e. further away from the heat sink than QW2. Also, each QW will have slightly different injection currents. This causes up to 0.5K difference in the carrier temperatures in the two wells. Figure 7.16 plots the electron temperature in each QW. As expected, it is slightly hotter than the LO-phonon temperature but follows the same shape.

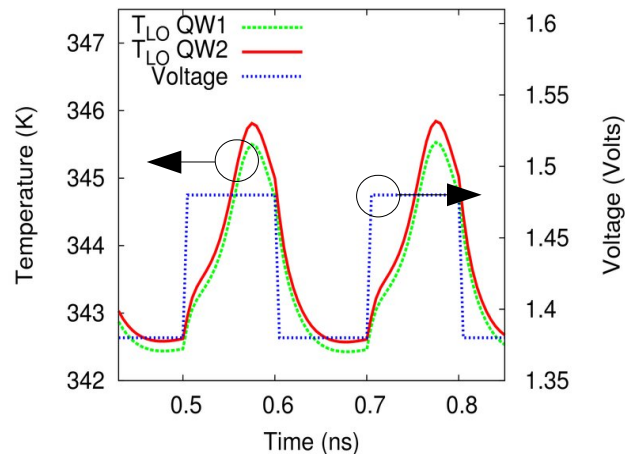


Figure 7.15: The temperature of the LO-phonon population in each QW.

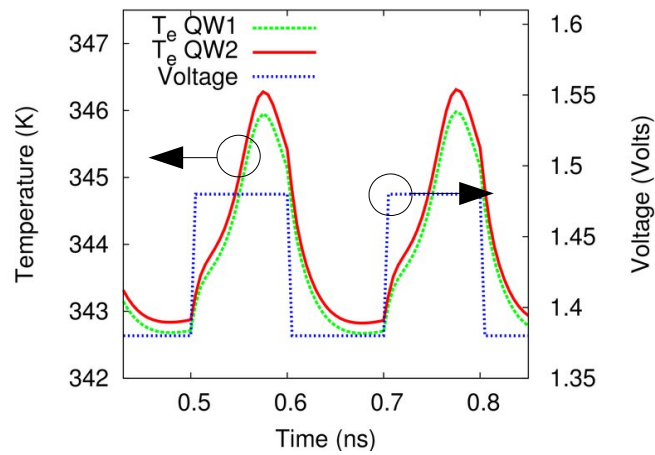


Figure 7.16: The electron temperature in each QW.

7.14 Summary

Within this chapter, a computationally efficient hot carrier/non-equilibrium LO-phonon model has been developed. The model eliminates many of the assumptions made in previously published more simple rate equation models, whilst holding on to their numerical attractiveness. Simplifications used in earlier models such as assuming the lasing energy is kT above the band edge have been replaced with

numerical results from non-parabolic band calculations using full Fermi-Dirac statistics. The lattice heat equation is solved in 2D along with the electron/hole/LO-phonon energy balance equations to obtain a four-temperature model of the QW. Using this newly developed simulation tool the impact of hot phonons on a 1.3 μ m edge-emitting dilute nitride laser has been investigated. The impact of the LO-phonon bottleneck has been found to be most significant under the ridge, where the injection current is largest. At moderate injection levels, the predicted output of the 1.3 μ m device decreases by ~1mW due to the hot carrier effect. At high injection currents, the inclusion of the hot phonon model decreases the predicted output power by up to 4mW. A super-linear divergence of the two predicted output powers is observed, indicating that including the hot-phonon model becomes more important the harder a device is driven. Modulation of the LO-phonon and QW carrier population temperatures is observed under high speed large-signal modulation. These temperature fluctuations are seen to change the position of the optical peak power and optical pulse shape.

The impact of hot phonons in dilute nitride devices is particularly large due to the large conduction band offset caused by the interaction of the conduction band wave function with the nitrogen level. In order to accurately model the modulation response and thermal roll-over in QW EELs, it is therefore essential to include hot phonon effects in device models.

7.15 References

- [1] J. Wang and H. Schweizer, "Nonlinear Gain Suppression in Quantum-Well Lasers Due to Carrier Heating: The Roles of Carrier Energy Relaxation, Electron-Hole Interaction, and Auger Effect", *IEEE Phot. Technol. Lett.*, 8,11, p. 1441, 1996
- [2] Chin-Yi Tsai et al. "Nonlinear Gain Coefficients in Semiconductor Quantum-Well Lasers: Effects of Carrier Diffusion, Capture, and Escape", *IEEE J. Sel. Top. Quant. Electron.*,1,2, p. 317,1995
- [3] Chin-Yi Tsai et al. "Hot carrier and hot phonon effects on high-speed quantum well lasers", *Appl. Phys. Lett.*, 63, 25, p. 3408, 1993
- [4] Chin-Yi Tsai et al. "Nonlinear Gain Coefficients in Semiconductor Lasers: Effects of Carrier Heating", *IEEE J. Quant. Electron.*, 32, 2, p. 201, 1996
- [5] S. F. Yu, "Dynamic Behavior of Vertical-Cavity Surface-Emitting Lasers", *J. of Quant. Electron.*,32, 7, p. 1169, 1996
- [6] Chin-Yi Tsai "Theoretical Modeling of the Small-Signal Modulation Response of Carrier and Lattice Temperature with the Dynamics of Nonequilibrium Optical Phonons in Semiconductor Lasers", *IEEE J. Sel. Quant. Electron.* 5, 3, p. 597, 1999
- [7] M. Grupen and K. Hess, "Simulation of Carrier Transport and Nonlinearities in Quantum-Well Laser Diodes", *IEEE J. Quant. Electron.*, 34, 1, p. 120, 1998
- [8] Yang Liu, "Numerical Investigation of Self-Heating Effects of Oxide-Confined Vertical-Cavity Surface-Emitting Lasers" , *IEEE Journal. Quantum. Electron.*, 41, 1 p. 15, 2005
- [9] Paul Harrison, "Quantum Wells, Wires and Dots Second Edition: Theoretical and Computational Physics of Semiconductor Nanostructures", Wiley, ISBN:0470010797, 2005

- [10] B.K. Ridley, "The electron-phonon interaction in quasi-two-dimensional semiconductor quantum-well structures", *J. Phys. C: Solid State Physics* 15, pp. 5889-5917, 1982
- [11] Ed. L. Challis, "Electron-Phonon Interactions in Low-Dimensional structures", Oxford University Press, ISBN: 0198507321, 2003
- [12] P.J. Bream, "Nonequilibrium carrier dynamics and gain in semiconductor quantum wells", PhD Thesis University of Nottingham, 2007
- [13] Chin-Yi Tsai et al., "Theoretical Modeling of the Small-signal Modulation Respose of Carrier and Lattice Temperatures with the Dynamics of Nonequilibrium Optical Phonons in Semiconductor Lasers" , *IEEE Sel. Top. Quant. Electron.*, 5, 3, p. 596, 1999
- [14] P.J. Bream, "Nonequilibrium carrier dynamics and gain in semiconductor quantum wells", PhD Thesis University of Nottingham, 2007
- [15] M. Grupen and K. Hess, "Simulation of Carrier Transport and non-linearities in QW Laser Diodes", *IEEE J. Q. Electron.* 34, 1, pp. 120-140, 1998